Sequential computations of two-dimensional temperature profiles and thermal stresses on an unstructured triangular mesh by GFVM method

Saeed Reza SabbaghYazdi[1,*], Tayebeh Amiri SaadatAbadi[2]

Received: January 2011, Accepted: June 2011

Abstract

In this research, a novel numerical algorithm is introduced for computation of temperature-induced before crack steady strain-stress field in plane-stress problem. For this purpose, two dimensional heat transfer equation and force equilibrium equations are sequentially solved using Galerkin Finite Volume method on identical unstructured triangular meshes when proper convergence for each field is achieved. In this model, a proper thermal boundary condition that is suitable for unstructured triangular meshes is introduced for analysis. Two test cases are used to assess accuracy of thermal and structural modules of the developed solver and the computed results are compared with theirs analytical solution. First, thermal analysis is performed for a rectangular plate which is connected to a supporting body with constant temperature and expose to surrounding liquid at three edges. Second, structural analysis is performed for a plate under distributed loads in two directions. Having obtained acceptable results from thermal and structural modules, thermal stress analysis is performed for a plate with fixed-end condition at one of edges, due to a uniform temperature field and the computational principle stress contours are compared with the Finite Element method results which have been reported in the literatures.

Keywords: Plane stress, Thermal stress, Galerkin finite volume method, Unstructured triangular mesh, Explicit solution.

1. Introduction

The unrestrained structural member expands or contracts in proportion to temperature variation freely. But the external and internal constraints often prevent the free movements of member and therefore, thermal stresses develop in the constrained structural member. The continuity of structural member and adjacent structures are example of the internal and external constraints. When these constraints limit the thermal strains, this limitation may cause to develop the tensile thermal stresses in structure. Since the tensile strength of concrete is low, the thermal cracking may occur due to thermal stresses [1].

Calculate the temperature and stress distribution is one of the important problems in solid mechanics. In the meantime the thermal stresses have a special place and theirs

important have motivated several researches and this phenomenon has modeled by various numerical techniques such as Finite Difference, Finite Element, etc, For example: temperature field calculation [2,3 and 4], stress distribution calculation [5,6 and 7], and calculation of thermal stress field [8].

In another research, the deformation of concrete which caused by the coupling effect of temperature and moisture has been simulated by the Finite Element method [9]. The long term deformation of concrete specimen containing silica fume subjected to constant load investigated experimentally as well as the stress redistribution between concrete and reinforcement as a result of time dependent behavior of concrete simulated theoretically [10]. The plain concrete simulated with the Plastic-Damage model by Finite Element method [11].

The Finite Volume method has been widely applied to heat transfer and fluid dynamics problems due to the relatively simple discretization procedure and conservative character in advection-diffusion problems have rendered the method attractive [12]. In recent decades, the Finite Volume method has been used for solution of temperature analysis, stress-

_____

* Corresponding Author: syazdi@kntu.ac.ir
1 Associate Professor, Civil Engineering Department of KNToosi University of Technology
2 PHD Candidate, Civil Engineering Department of KNToosi University of Technology

strain computations and thermal stress solution of solid mechanic problems that some of them are reviewed in the following paragraphs.

In one research, an unstructured Finite Volume node centered formulation, implemented using an edge-based data structure for the solution of two-dimensional potential problems [13]. Lyra et al have used an edge-based unstructured Finite Volume procedure for the thermal analysis for steady state and transient problems [14]. Recently, the explicit Galerkin Finite Volume method has been used to compute temperature field as a result of the cement hydration heat in young mass concrete on structured triangular meshes [15].

Wheel introduced an implicit Finite Volume method for determining the displacement fields and elastic stress distributions in structures that have axisymmetric geometries using structured meshes [16]. Oliveira et al used the Finite Volume method for solution of the static and transient problems in the structural mechanics field. Although an implicit time stepping technique was used for the analysis, the source term is treated explicitly on the structured meshes [17]. Wenke et al presented a Finite Volume based discretization method for determining displacement, strain and stress distributions in two dimensional structures on unstructured meshes. They incorporate rotation variables in addition to the displacement degrees of freedom [18]. Vaz Jr et al were focused on the application of the Finite Volume method to solid mechanics using implicit time stepping for structured meshes and evaluated the method accuracy to calculate the stress field in solids [12]. Recently, a model has been developed to compute the stress-strain fields for plane strain problems using an explicit formulation of Galerkin Finite Volume method [19].

Demirdzić et al presented a Finite Volume method for prediction of stresses and displacements in Thermo-Elasto-Plastic Material. They performed the analysis on the structured meshes and used an explicit time stepping technique for their time dependent analysis [20]. Demirdzić et al extended their numerical technique for the stress analysis in isotropic bodies subjected to Hygro-Thermo-Mechanical loads. In this research, the temperature, stress, displacement and humidity fields are calculated using the fully implicit time differencing whereas the source term and diffusion fluxes are treated explicitly [21]. Fainberg et al performed similar work for Thermo-Elastic material [22].

In present research, 2D matrix free Galerkin Finite Volume solution is utilized for computing combined temperature and stress-strain fields on the same unstructured linear triangular elements. The proper and suitable technique for unstructured triangular meshes is developed and implemented for boundary conditions associate with the heat transfer and force equilibrium equations. In this combined numerical model, after converging the temperature field computations, the convergence of the force equilibrium equations are achieved. Both computations for governing equations of temperature and stress-strain fields (in the absence of source terms) are performed on a certain unstructured triangular mesh via some explicit iteration. Since the thermal stress analysis in this paper is performed for steady state problems, the thermal stresses are computed using the thermal strains which are accumulatively calculated from the results of thermal analyses.

Accuracy of the two thermal and structural modules of the introduced numerical model is assessed by comparison of computational results of temperature fields due to various boundary conditions and stress-strain fields due to external loads with available analytical solutions of two benchmark cases. Finally, the application of the combined model is presented by computation of steady state distribution of thermal stress in a clamped plate subjected to uniform temperature field and the computed results of principal thermal stress are compared with the solutions of Finite Element method which have been reported by the previous researchers [23, 24].

2. Constitutive Model

2.1. Thermal Model

The heat transfer equation is extracted from different thermodynamics and heat transfer references as following equation [25]:

$$\rho C \dot{T} = K(\nabla^2 T) + \dot{Q} \tag{1}$$

Where K is the thermal conductivity of concrete, T is the concrete temperature, $\dot{Q}$ is the rate of heat generation per unit volume, ρ is the material's density and C is the material's specific heat.

The two main thermal boundary conditions in thermal analysis are as follow:

$$T = T_0 \quad , \quad K.\frac{dT}{dn} = -q \tag{2}$$

Where T_0 and q are the air temperature and rate of heat exchange.

$$q = \pm q_c + q_r - q_s \tag{3}$$

Where q_c, q_r and q_s are heat flux by convection, long wave radiation and solar radiation [26].

2.2. Elastic Model

Cauchy's equation is known as the governing equation for solid mechanics and is attained from equilibrium equation. This equation can be used to solve the structural problems and compute the stress-strain field [19].

The Cauchy's equation in the absence of body force is written as follows:

$$\begin{cases} \rho \ddot{u}_x = \dfrac{\partial \sigma_{xx}}{\partial x} + \dfrac{\partial \sigma_{xy}}{\partial y} \\ \rho \ddot{u}_y = \dfrac{\partial \sigma_{xy}}{\partial x} + \dfrac{\partial \sigma_{yy}}{\partial y} \end{cases} \tag{4}$$

Where $\ddot{u}_i$ is the body acceleration in i direction ($i=x,y$).

The stress field for plane stress problem is expressed as follows:

$$\sigma_{xx} = C_{11}\varepsilon_{xx} + C_{12}\varepsilon_{yy}$$

$$\sigma_{yy} = C_{21}\varepsilon_{xx} + C_{22}\varepsilon_{yy}$$

$$\sigma_{xy} = \sigma_{yx} = C_{33}\varepsilon_{xy} \tag{5}$$

$$C = \frac{E}{(1-\vartheta^2)}\begin{bmatrix} 1 & \vartheta & 0 \\ \vartheta & 1 & 0 \\ 0 & 0 & \frac{1-\vartheta}{2} \end{bmatrix}$$

Where C is the stiffness matrix. The strain field is expressed in terms of displacement components as follows:

$$\varepsilon_{xx} = \frac{\partial u_x}{\partial x} + \varepsilon_T \tag{6}$$

$$\varepsilon_{yy} = \frac{\partial u_y}{\partial y} + \varepsilon_T$$

$$\varepsilon_{xy} = \frac{\partial u_x}{\partial y} + \frac{\partial u_y}{\partial x}$$

Where ε_T is the thermal strain and is calculated from "equation (7)":

$$(\varepsilon_T)_n = \alpha\Delta T = \alpha\left(T^{t+\Delta t}{}_n - T^t{}_n\right) \tag{7}$$

Where α is the coefficient of thermal expansion and $T_n{}^t$ is the temperature of node n at time t.

3. Numerical simulation

A numerical program is developed to simulate the thermal stress of member a time before crack. This program is compiled in the format of FORTRAN code. Each node of element has 2 freedoms corresponding to the 2 displacement of that node.

3.1. Finite Volume

3.1.1. Thermal Model
Heat transfer equation is written as "equation (8)":

$$\dot{T} + (\nabla.F^T) = S^T \tag{8}$$

Where

$$S^T = \frac{\alpha}{K}\dot{Q}(t_e) \quad , \quad F^T = F_x^T\hat{\imath} + F_y^T\hat{\jmath} \tag{9}$$

In which $F_i^T = \alpha\frac{\partial T}{\partial x_i}, (i = x, y)$

Application of the variational method, after multiplying the residual of the above equation by the test function ϕ and integrating over a sub-domain, the "equation (8)" is written as "equation (10)":

$$\int_\Omega (\dot{T})\phi d\Omega + \int_\Omega (\nabla.F^T)\phi d\Omega = \int_\Omega (S^T)\phi d\Omega \tag{10}$$

Considering the test function ϕ as the shape function of central node of a sub-domain formed by gathering linear triangular meshes, the above equation is expressed as follows:

$$\int_\Omega (\dot{T})\phi d\Omega = \int_\Omega (F^T.\nabla\phi)d\Omega + \int_\Omega (S^T)\phi d\Omega \tag{11}$$

The value of the shape function (ϕ) is equal to unit at a desired node n, and zero at the other neighboring nodes k for each triangular element. Using the properties of the linear shape function of triangular elements, following approximations can be made to discretize the terms in the above equation:

$$\frac{\partial}{\partial t}\int_\Omega \phi T d\Omega \approx (\dot{T})_n \frac{\Omega_n}{3} \tag{12}$$

$$\int_\Omega (F^T.\nabla\phi)d\Omega \approx -\frac{1}{2}\sum_{m=1}^{3}(F^T.\Delta l)_m$$

$$\int_\Omega (S^T)\phi d\Omega \approx \frac{\Omega_n}{3}.S_n^T$$

Considering counterclockwise direction for the contour integrals in each triangular element, only external faces of the sub-domain (edges k opposite to its central node n) remain effective in the resulting formulation.

$$\Omega_n(\dot{T})_n = \Omega_n S_n^T - \frac{3}{2}\left[\sum_{k=1}^N (F^T.(\Delta l))_k\right]_n \tag{13}$$

Using Finite Differencing for the first order time derivative term,

$$\Omega_n(\dot{T})_n = \left(\frac{T^{t+\Delta t}-T^t}{\Delta t}\right)_n \Omega_n \tag{14}$$

The explicit discrete form of heat diffusion equation for sub-domain Ω (Fig.1) is expressed as:

$$T_n{}^{t+\Delta t} = T_n{}^t + (\Delta t)_n^t\left[S_n^T - \frac{3}{2\Omega_n}\left[\sum_{k=1}^N (F^T.(\Delta l_i))_k\right]_n\right]^t$$
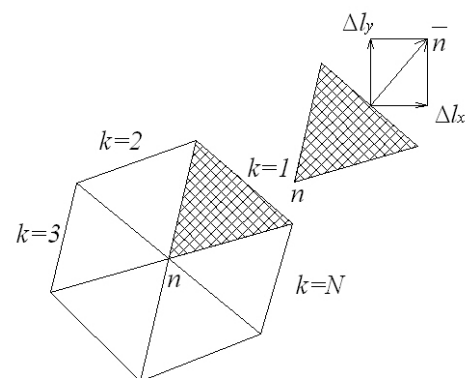
$$i=(x,y) \tag{15}$$

Fig. 1. Triangular elements within the sub-domain Ω_n for temperature computation

Where $T_n{}^{t+\Delta t}$ is the temperature of node n at $t+\Delta t$ time, N is the boundary edges number of sub-domain and Δl_i is the i direction component of the normal vector for boundary edge k of sub-domain.

Note that, the time step Δt in above temperature computation formulation is a parameter that helps stabilize explicit time marching and can be considered to be the local time step $(\Delta t)^t{}_n$.

In order to compute the components of heat flux vector, $F^T = F_x^T \hat{\imath} + F_v^T \hat{\jmath}$ must be calculated at the center of elements corresponding to boundary edges of the sub-domain as following equation:

$$\left(F_x^T\right) = \left(\alpha \frac{\partial T}{\partial x}\right) \approx \frac{1}{\Omega_n} \sum_{m=1}^{3} \left(\bar{T}.\Delta l_y\right)_m \tag{16}$$

$$\left(F_y{}^T\right) = \left(\alpha \frac{\partial T}{\partial y}\right) \approx \frac{1}{\Omega_n} \sum_{m=1}^{3}(\bar{T}.\Delta l_x)_m$$

3.1.2. Elastic Model

The two dimensional Cauchy's equation in i direction is expressed as follows:

$$\rho(\ddot{u}_\iota) = \nabla.F_i{}^S \, (i = x, y)$$

$$\text{Where,} \quad F_i^S = \sigma_{ix}\hat{\imath} + \sigma_{iy}\hat{\jmath} \tag{17}$$

Application of the variational method, after multiplying the residual of the above equation by the test function ϕ and integrating over a sub-domain Ω the above equation is written as follows:

$$\int_\Omega \phi\rho(\ddot{u}_\iota)\,d\Omega = \int_\Omega \phi\left(\nabla.F_i{}^S\right) \tag{18}$$

Considering the test function ϕ as the shape function of central node of a sub-domain formed by gathering linear triangular meshes (Fig. 2), the above equation is expressed as follows:

$$\int_\Omega \phi\rho(\ddot{u}_\iota)\,d\Omega = -\int_\Omega \left(F_i{}^S.\nabla\phi\right)d\Omega \tag{19}$$

The value of the shape function (ϕ) is equal to unit at a desired node n, and zero at the other neighboring nodes k for each triangular element. Using the properties of the linear shape
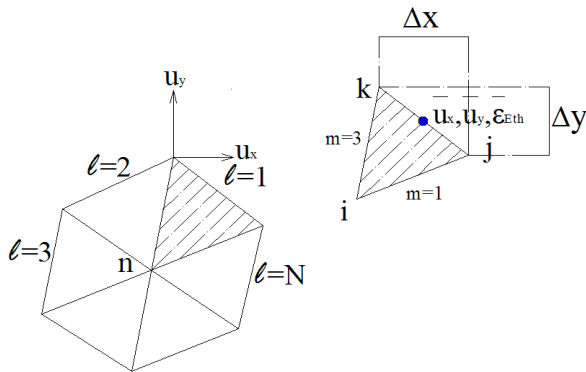

Fig. 2. Triangular elements within the sub-domain Ω_n for stress-strain computations

function of triangular elements, following approximations can be made to discretize the terms in the above equation:

$$\rho \frac{\partial^2}{\partial t^2} \int_A \phi u_i d\Omega \approx \rho \frac{\Omega_n}{3}(\ddot{u}_\iota)$$

$$\int_A (F^S.\nabla\phi)d\Omega \approx -\frac{1}{2}F^S \sum_{m=1}^{3}(\Delta l)_m \tag{20}$$

$$\int_A \phi.S_i^S d\Omega = \frac{1}{3}S_i^S \Omega_n$$

Considering counterclockwise direction for the contour integrals in each triangular element, only external faces of the sub-domain (edges k opposite to its central node n) remain effective in the resulting formulation.

$$\rho\Omega_n(\ddot{u}_\iota)_n = \Omega_n\left(S_i^S\right)_n + \frac{3}{2}\left[\sum_{l=1}^{N}\left(F_i^S.(\Delta l_i)\right)_l\right]_n \tag{21}$$

The time derivative term of equation can be written as the following equation:

$$\rho\Omega_n(\ddot{u}_\iota)_n = \rho\Omega_n\left(\frac{u_i{}^{t+\Delta t}-2u_i{}^t+u_i{}^{t-\Delta t}}{(\Delta t)^2}\right)_n \tag{22}$$

The discrete form of the Cauchy's equation is written as follows:

$$\left(u_i{}^{t+\Delta t}\right)_n = 2(u_i)_n{}^t - (u_i)_n{}^{t-\Delta t} + (\Delta t^2)_n^t\left(\frac{3}{2\rho\Omega_n}\right)\left[\sum_{l=1}^{N}\left(F_i^S.(\Delta l)_i\right)_l + \frac{1}{3\rho}S_i^S\right]_n^t$$

$$, (i=x,y) \tag{23}$$

Where $\left(u_i{}^{t+\Delta t}\right)_n$ is the displacement of node n at $t+\Delta t$ computational stage in i direction. Note that, the time step Δt in above strain analysis formulation is a parameter that helps stabilize explicit iterative computations toward the equilibrium condition and can be considered to be the local time step $(\Delta t)_n^t$. The components of the $F_i^S = \sigma_{ix}\hat{\imath} + \sigma_{iy}\hat{\jmath}$ are computed from

$$\sigma_{xx} = \left\{C_{11}\left(\frac{\partial u_x}{\partial x} + \bar{\varepsilon}_T\right) + C_{12}\left(\frac{\partial u_y}{\partial y} + \bar{\varepsilon}_T\right)\right\}$$

$$\sigma_{xx} \approx \left\{\frac{1}{\Omega_n}\sum_{m=1}^{3}\left(C_{11}\bar{u}_x\Delta y - C_{12}\bar{u}_y\Delta x + \bar{\varepsilon}_T(C_{11}+C_{12})\right)_m\right\}$$

$$\sigma_{yy} = \left\{C_{12}\left(\frac{\partial u_x}{\partial x} + \bar{\varepsilon}_T\right) + C_{11}\left(\frac{\partial u_y}{\partial y} + \bar{\varepsilon}_T\right)\right\} \tag{24}$$

$$\sigma_{yy} \approx \left\{\frac{1}{\Omega_n}\sum_{m=1}^{3}\left(C_{12}\bar{u}_x\Delta y - C_{11}\bar{u}_y\Delta x + \bar{\varepsilon}_T(C_{12}+C_{11})\right)_m\right\}$$

$$\sigma_{xy} = \sigma_{yx} = \left\{C_{22}\left(\frac{\partial u_x}{\partial y} + \frac{\partial u_y}{\partial x}\right)\right\}$$

$$\sigma_{xy} = \sigma_{yx} \approx \left\{\frac{1}{\Omega_n}\sum_{m=1}^{3}\left(C_{22}\bar{u}_y\Delta y - C_{22}\bar{u}_x\Delta x\right)_m\right\}$$

Where $\bar{\varepsilon}_T$ is the average thermal strain for 2 nodes of each edge, Ω_n is the area of triangular element, N is the number of triangle edge. The coefficient C_{ij} is ij component of stiffness matrix.

4. Boundary Condition

4.1. Thermal Model

Two types of thermal boundary conditions are usually applied in this numerical modeling which the essential and natural boundary conditions are used for specified temperature and temperature gradient flux at boundaries.

4.1.1. Specified Temperature
It is easy impose this boundary condition in the numerical techniques. The computed temperature of each node is replaced to the specified temperature.

4.1.2. Temperature Gradient
In order to impose the given normal temperature gradient to the boundary edges (G), the unit normal vector of the boundary edges $n=(n_x, n_y, n_z)$ can be utilized to compute $G=(Gn_x, Gn_y, Gn_z)$ at the desired boundaries. A simple technique can be used for the cases that the boundary normal vector is parallel to one of the main directions of coordinate system. The computational difficulties arise for the inclined or curved boundaries. To overcome this problem, the computed gradient flux vector ("equation (25)"), at the centre of adjacent elements (Hatched elements in Fig. 3) may be modified at the end of each computational step as "equation (27)".

$$\bar{F}^T = (F^T)_x \hat{\imath} + (F^T)_y \hat{\jmath} \rightarrow \bar{F}^T = \left(\frac{\partial T}{\partial x}\right)\hat{\imath} + \left(\frac{\partial T}{\partial y}\right)\hat{\jmath} \tag{25}$$

$$(\bar{G})_{normal} = \left(\frac{H(T_{surface}-T_{air})}{k}n_x\right)\hat{\imath} + \left(\frac{H(T_{surface}-T_{air})}{k}n_y\right)\hat{\jmath} \tag{26}$$

$$(\bar{F}^d)_{modify} = \left(\frac{\partial T}{\partial x} + \frac{H(T_{surface}-T_{air})}{k}n_x\right)\hat{\imath} + \left(\frac{\partial T}{\partial y} + \frac{H(T_{surface}-T_{air})}{k}n_y\right)\hat{\jmath} \tag{27}$$

4.2. Elastic Model

Four sets of boundary conditions are commonly simulate the employed constraints in experiments which are represented as follows:
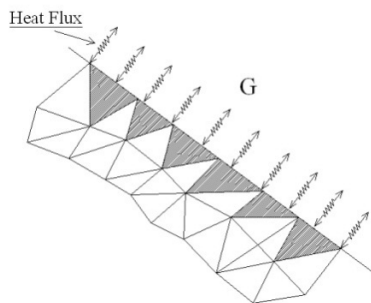

Fig. 3. Triangular elements of boundary edge

4.2.1. Fixed-End
In this boundary condition, the rotation and displacements are limited (Fig.4).

$$u_x = 0, u_y = 0, \theta = 0 \tag{28}$$

4.2.2. Pinned-End
In this state, all transitional freedoms are prevented but rotational freedoms are free.

$$u_x = 0, u_y = 0 \tag{29}$$

4.2.3. Sliding-End
The normal displacement of boundary isn't allowed and only the tangential displacement is free.

$$u_{normal} = 0, \theta = 0 \tag{30}$$

5. Time Integration
The Time step of both equations (heat transfer equation and force equilibrium equation) is computational time step and is used to achieve convergence of temperature and stress - strain field.

5.1. Thermal Model

K is the index of concrete temperature transition capability and C is the index of required heat amount for temperature change of One degree Celsius per unit mass. If the propagation speed of heat is considered proportional to α_n, the maximum value for the time step of the heat diffusion equation can be considered as "equation (31)":

$$\Delta t < \frac{1}{M}\left(\frac{\Omega_n}{\alpha_n}\right), \alpha_n = \left(\frac{K}{\rho C}\right)_n \tag{31}$$

Where M is the proportion coefficient which its value can be considered more than one.
For the steady state problem, by using the particular time step for each node, the execution time is reduced which this concept is known as local time stepping method.

5.2. Elastic Model

In order to have stable explicit solution, the Courant's number must be less than 1. According to proposed relation from reference [19], the time step has been limited to
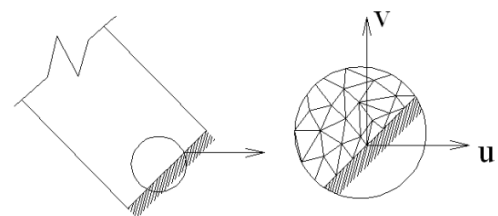

Fig. 4. Clamped constraint

following amount:

$$\Delta t_n < \frac{r_n}{s_t} \tag{32}$$

The parameter r_n is ratio of area to perimeter in each control volume.

$$r_n = \frac{\Omega_n}{P_n} \quad , \quad P_n = \sum_{k=1}^{Nedge}(\Delta l)_k \tag{33}$$

Where Ω_n and P_n is area and perimeter of the control volume, respectively.

s_t is the speed of information transition which is calculated from "equation (34)":

$$s_t = \sqrt{\frac{E}{\rho(1-\vartheta^2)}} \tag{34}$$

The time step of each node is different from others nodes. Using the concept of local time stepping method,the speed of convergence to equilibrium condition rises.

6. Verification

In this section, two test cases are used to assess the accuracy of both thermal and structural modules of the present model and after ensure the accuracy of results, the application test is presented. All the computations are performed using a computer with Intel Core2Duo T7100 1.8GHz CPU, with 2 GB RAM memory, and in order to assess the performance of the present Finite Volume solver, the CPU time was measured for computations.

6.1. Thermal Analysis

6.1.1. A Plate surrounded by a Liquid

A rectangular plate which is connected to a supporting body and expose to surrounding liquid at three edges is considered in this section (Fig. 5). Constant temperature (T_b) is considered at the fixed support and the surrounding liquid assumed to have constant temperature(T_∞).

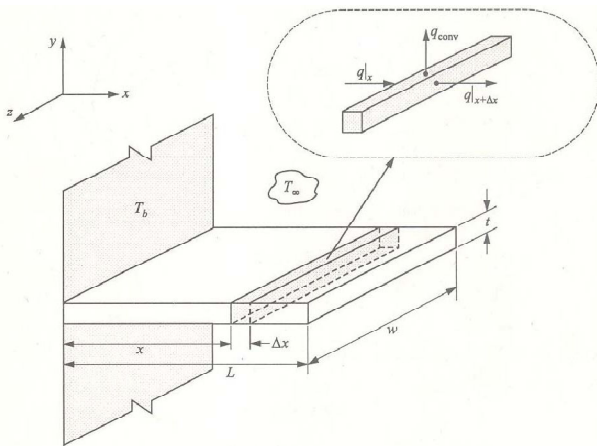The developed solver is utilized to perform thermal analysis

Fig. 5. Schematic illustration of thin plate surrounded by ambient liquid fixed to a rigid body at one edge

in x-y plane. The rate of heat exchange at three edges which are exposed to the ambient liquid can be represented as follows [27]:

$$q|_x = -KA\frac{dT}{dx}\Big|_x \; , q|_{x+\Delta x} = -KA\frac{dT}{dx}\Big|_{x+\Delta x} \; , q_{conv} = \bar{h}(P.\Delta x)(T - T_\infty) \tag{35}$$

Where K, A, P and $\bar{h}$ are thermal conductivity, cross section area and perimeter of the desired element and the heat transfer coefficient,respectively.

The theoretic solution of this problem with represented boundary conditions is expressed as following equation:

$$\frac{\theta}{\theta_b} = \frac{\cosh[n(L-x)]+\left(\bar{h}/nK\right)\sinh[n(L-x)]}{\cosh(nL)+\left(\bar{h}/nK\right)\sinh(nL)} \; , \quad \theta_b = T_b - T_\infty \tag{36}$$

Where L and x are the maximum length of the plate in plane of the analysis and desired distance from support which has been shown in Fig. 5.

For a thin plate:

$$n \approx \sqrt{\frac{2\bar{h}}{Kt}} \tag{37}$$

Where t is the thickness of the plate.

The computed temperature contours are shown in Fig. 6 and the computed temperatures with theoretic results are compared in Fig. 7 The root mean square of the computed temperature is shown in Fig. 8.

6.2. Stress Analysis

6.2.1 A Plate Subjected to Distributed Loads

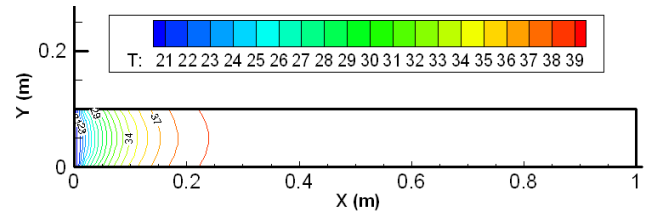In this test case the applied loads to a 10cm×10cm×1cm plate

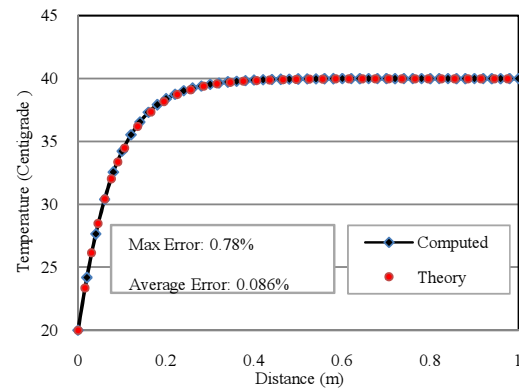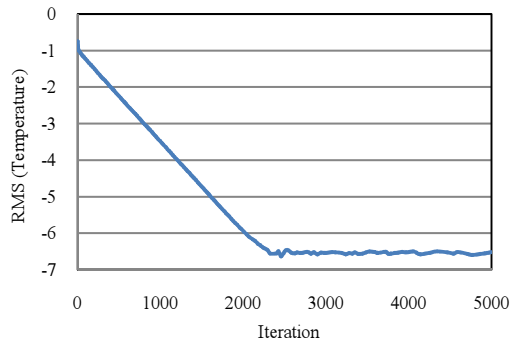**Fig. 6.** Computed temperature contours (°C)

Fig. 7. Comparison of computed temperature with theoretic results

Fig. 8. Convergence of the logarithm of root mean square of the temperature

are given as distributed loads in two directions (Fig. 9). For this test case in which no body force exists, the displacement and principal stressesare compared with analytical solutions [28].

The relative displacements of plate edges can be obtained from following relation [28]:

$$u_x = \varepsilon_{xx} * l \quad , \quad u_y = \varepsilon_{yy} * l \qquad (38)$$

Where l is dimension of plate and ε_{xx} ,ε_{yy} is stain at x, y direction, respectively and are calculated from "equation (39)".

$$\varepsilon_{xx} = \frac{1}{E}(\sigma_{xx} - \vartheta\sigma_{yy}) \quad , \quad \varepsilon_{yy} = \frac{1}{E}(\sigma_{yy} - \vartheta\sigma_{xx}) \qquad (39)$$

Where E is Young's modulus and υ is the Poisson's ratio (Table.1). With the specified plate conditions, the x and y directions displacements are analytically computed as
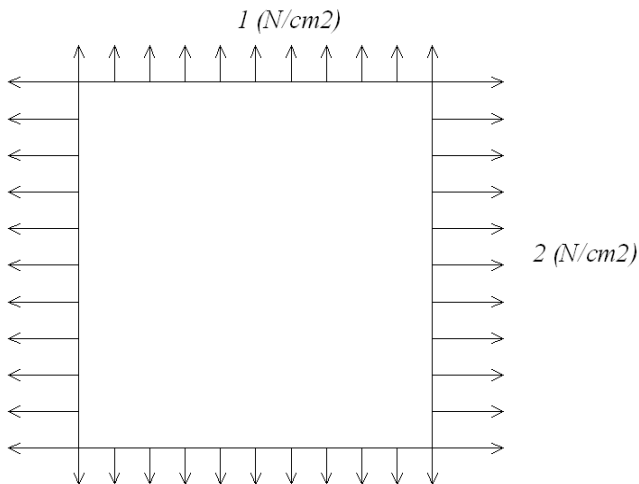
Fig. 9. Schematic illustration of a plate under distributed loads in two directions

Table 1. Plate specification

Characteristic	Value	Characteristic	Value
Thickness	1 cm	Young 's modulus, E	10 MPa
Density, ρ	2600 kg/m^3	Poisson's ratio, ϑ	0.33

$+0.0167m$ and $-0.0034m$, respectively.

Standard type Finite Element method structural solvers require extra structural constraints to stabilize the solution procedure (Fig. 10).

The presented Finite Volume method has the ability to solve the problems without any extra structural constraints. The following problem is analyzed without any structural constraint using the developed Finite Volume method:

Fig.11 shows the unstructured meshes used for the present Finite Volume computations. The direction computed displacement in x and y directions are presented as follows:

$$u_x = 16.699 * 10^{-3} cm$$
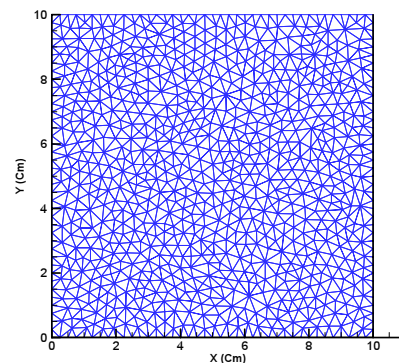
$$u_y = 3.365 * 10^{-3} cm \qquad (40)$$

The typical computed color coded maps of displacements are presented in Fig. 12 (a, b).

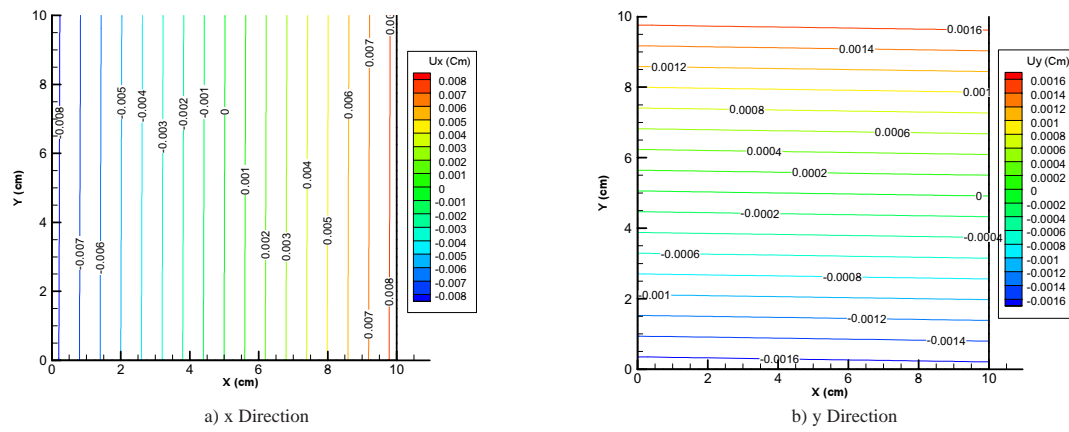The maximum and minimum principal stresses are calculated from "equation (41)":

$$\sigma_{max,min} = \left(\frac{\sigma_{xx}+\sigma_{yy}}{2}\right) \pm \sqrt{\left(\frac{\sigma_{xx}-\sigma_{yy}}{2}\right)^2 + \sigma_{xy}^2} \qquad (41)$$
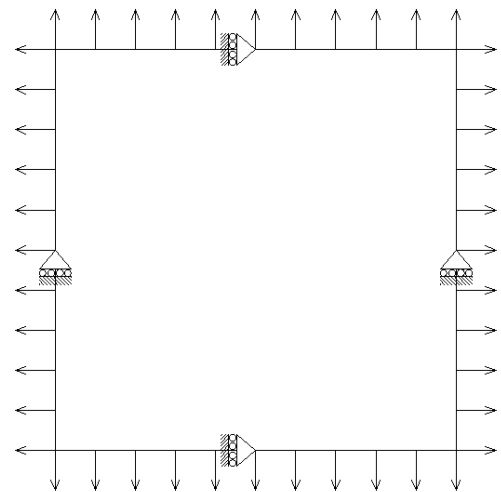
Fig. 10. Virtual constraints required for Finite Element solution

Fig. 11. Unstructured meshes for stress analysis (With 927 nodes and 1692 elements)

a) x Direction   b) y Direction

Fig. 12. Displacement contours (unit: cm)

Where σ_{xx}, σ_{yy} and σ_{xy} are in x,y directions and shear stresses, respectively.

The different triangular mesh refinements are used for sensitivity analysis of the developed model which are shown in Fig. 13 (*a,b,c*), whereas Fig. 14 (*a,b*) represent converged displacement in *x,y* directions for different meshes refinements with the measures CPU times.

6.3. Thermal Stress Analysis

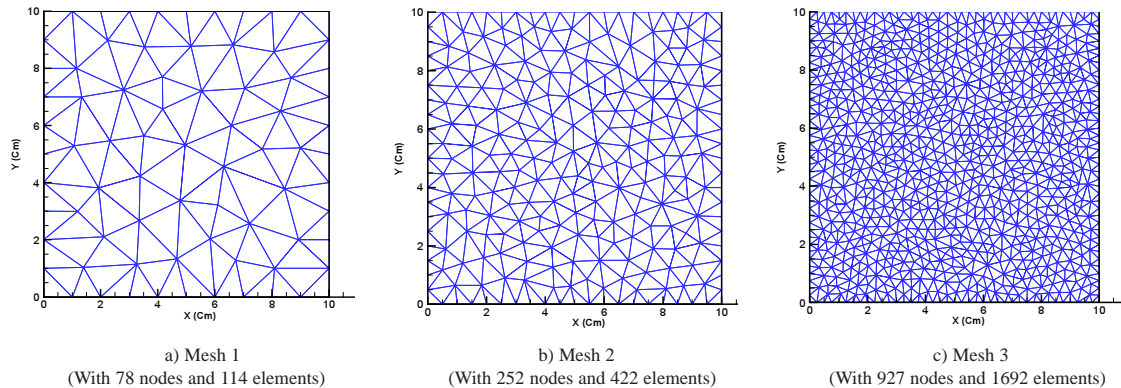*6.3.1. A Fixed Edge plate Subjected to Temperature Changes*
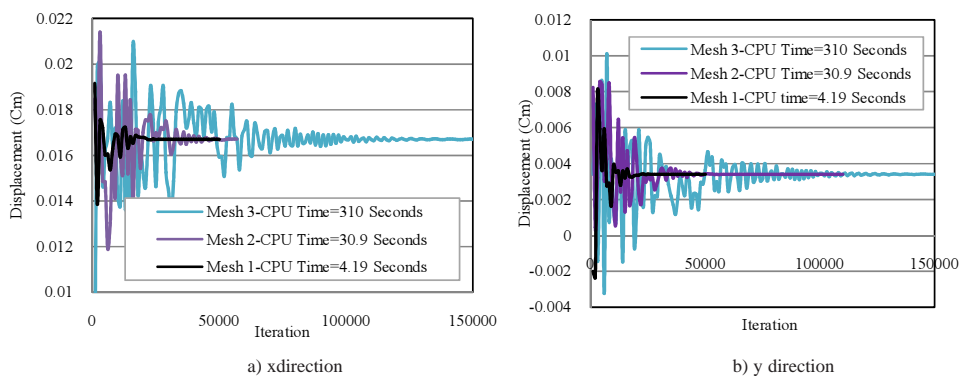
The external thermal stresses are created because of

the difference between the coefficients of thermal expansion of body and its adjacent structures. When temperature difference in body and its adjacent structures is equal, the thermal strains in body and its adjacent structures are different because of the difference between their coefficients of thermal expansion, so the thermal stresses are created.

A plate specimen is clamped at the left and is subjected to a uniform temperature of $50°C$ which is shown in Fig. 15 [23]. Material specifications are shown in Table .2.

In the previous researches, The T-MFPA and ALGOR commercial softwares based on Finite Element method were used for thermal analysis. Under a uniform
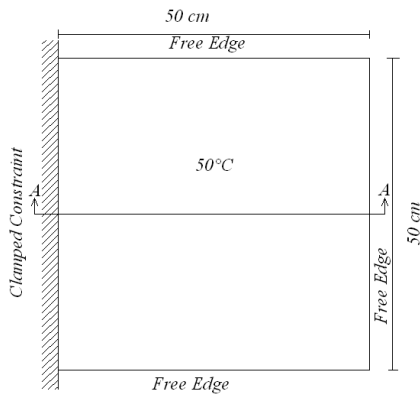

a) Mesh 1
(With 78 nodes and 114 elements)

b) Mesh 2
(With 252 nodes and 422 elements)

c) Mesh 3
(With 927 nodes and 1692 elements)

Fig. 13. Different mesh refinements for stress analysis

a) xdirection   b) y direction

Fig. 14. Convergence behavior of computed displacements forDifferent mesh refinements

Fig. 15. Schematic illustration of a plate clamped at the left and subjected to a uniform temperature

Table 2. Plate specification

Characteristic	Value	Characteristic	Value
Length	50 * 50 cm	Temperature difference	50 ℃
Yong 's modulus	210 Gpa	Coefficient of thermal expansion	$\alpha = 1.2E-5/{}_{\circ C}$
Poisson 's ratio	$\vartheta = 0.3$		

temperature, thermal stresses are created due to the restraint boundary conditions. The computed stress fields by ALGOR and T-MFPA softwares [23,24] are shown in Fig. 16 (a,b).

In order to assess the sensitivity of present model, various triangular meshes are used which Fig. 17, 18 represent the meshes and associated computed c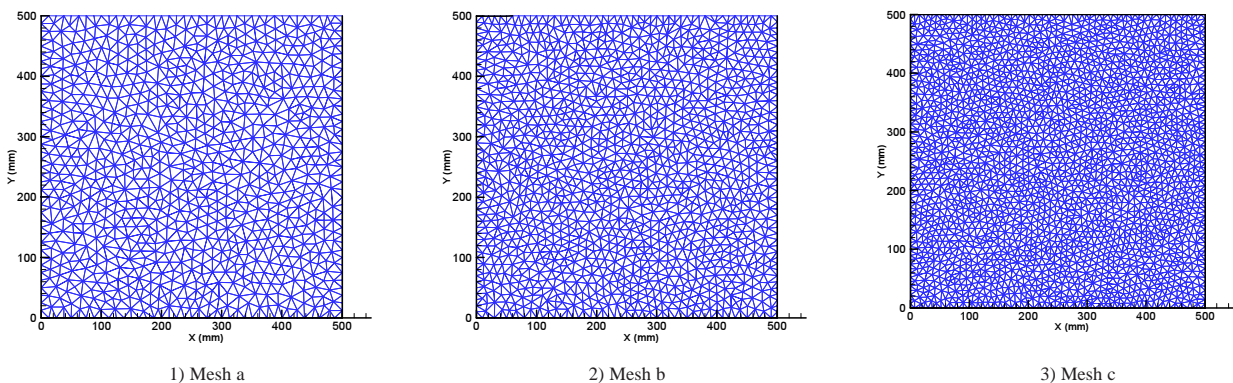ontours of maximum principal stress. The values of maximum principal stress along x direction (section A-A in Fig. 15) which are computed by the present Finite Volume model are extracted and compared with results obtained from results of two Finite Element model that were reported in references (23 and 24) in Fig. 19 and the differences are tabulated in Table.3.

In order to provide a better understanding about the effects of gradual load imposing technique, the convergence behavior of the computed displacements is shown in Fig. 20 and the root mean square of the computed displacements is shown in Fig. 21.
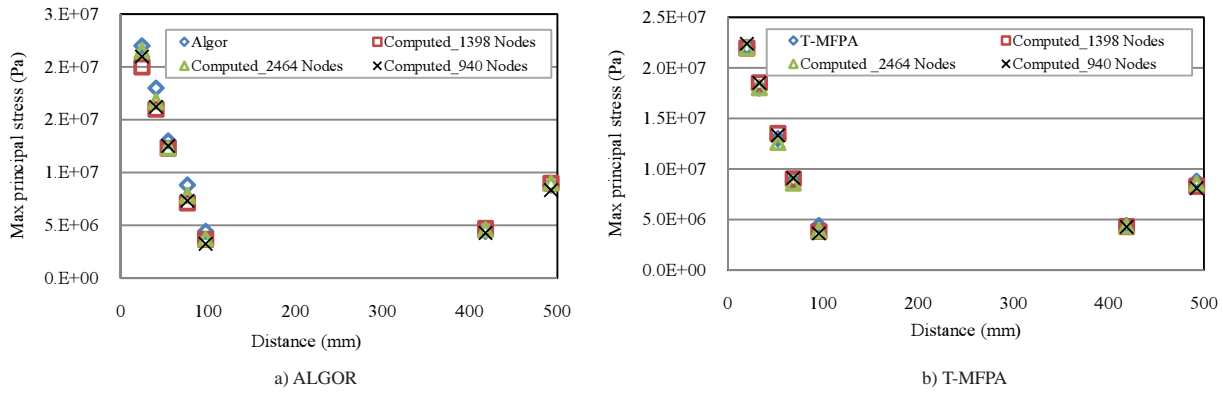

a) T-MFPA [21]

b) ALGOR [20]
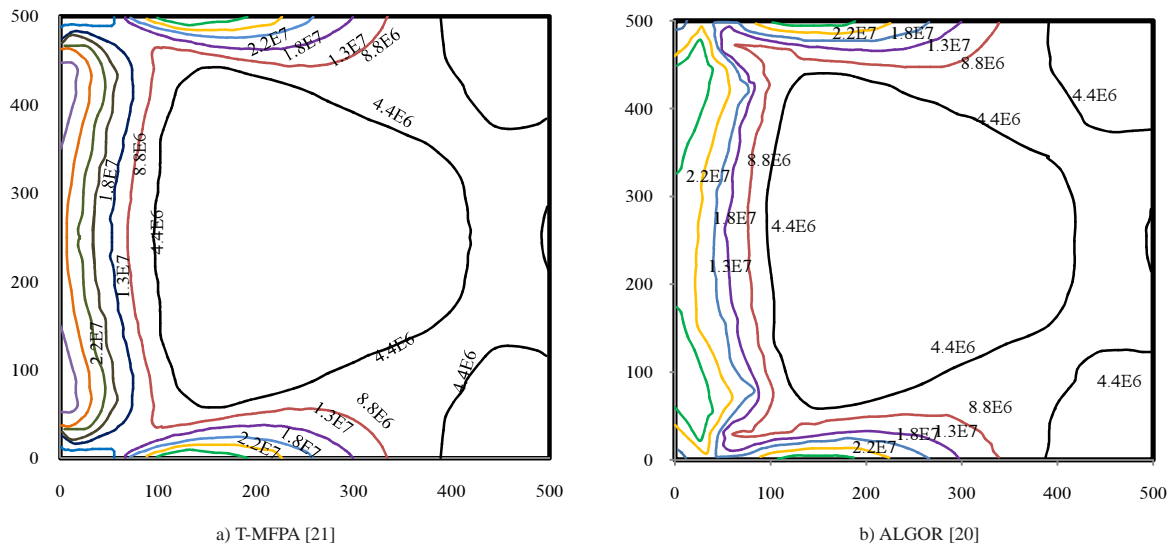
Fig. 16. Maximum principal stress contours by Finite Element Method soft wares

1) Mesh a

2) Mesh b

3) Mesh c

Fig. 17. Unstructured triangle mesh for thermal stress analysis

| 1) Mesh a | 2) Mesh b | 3) Mesh c |
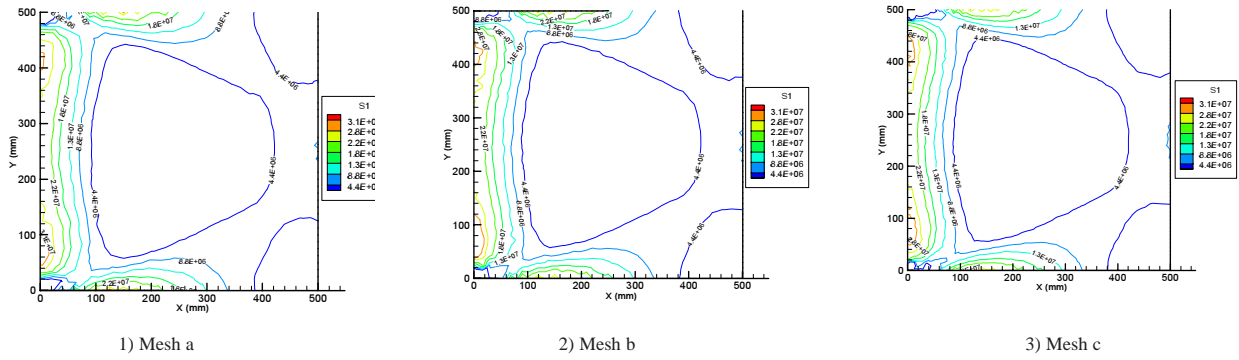
Fig. 18. Maximum principal stress contours computed by the developed model

| a) ALGOR | b) T-MFPA |

Fig. 19. Comparison of section A-A Stresses with results of Finite Element Method

Table 3. Comparison of computed results for various meshes with Finite Element results

| Mesh | Number of nodes | Number of elements | Displacements of the free end (m) | | Average difference between the results (%) | | | | | | CPU time (second) |
					Displacement				Principal stress		
					ALGOR [23]		T-MFPA [24]		ALGOR [23]	T-MFPA [24]	
			Δx	Δy	Δx	Δy	Δx	Δy			
ALGOR [23]	-------	-------	$3.076E-4$	$1.55E-4$	----	----	---	---	-------	-------	-------
T-MFPA [24]	-------	-------	-------	-------	----	----	---	---	-------	-------	-------
Present GFV model	a	940	1718	$3.16E-4$	$1.51E-4$	2.73	2.76	---	---	10.09	5.51	130.9
Present GFV model	b	1398	2594	$3.15E-4$	$1.52E-4$	2.40	2.12	---	---	10.08	4.43	250.5
Present GFV model	c	2464	4658	$3.14E-4$	$1.53E-4$	2.08	1.48	---	---	6.89	3.00	311.6

7. Conclusions

In this work, a matrix free solver is presented to compute the temperature-induced steady strain-stress field a time before crack in plane-stress problem. The Galerkin Finite Volume method for unstructured triangular elements is used for iterative solution of both temperature and force equilibrium equations on a certain mesh. In this method, the shape function free discrete forms of governing equations can be explicitly solved for every single node at each computational step. In this research, proper boundary conditions are introduced for temperature analysis and stress-strain computations on unstructured linear triangular meshes to implement heat as well as load and constraints boundary conditions.

The thermal and structural modules of the developed model are checked and their result's accuracies are assessed by comparing with the analytical solutions of two bench marks. First the unidirectional temperature filed in a thin plate which

S. R. Sabbagh Yazdi, T. Amiri SaadatAbadi
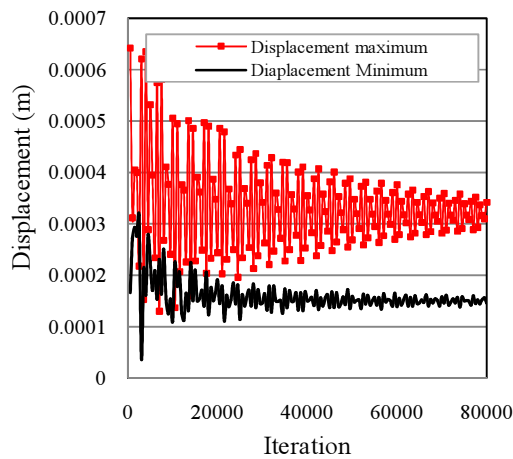
Fig. 20. Convergence of the logarithm of root mean square of the displacements
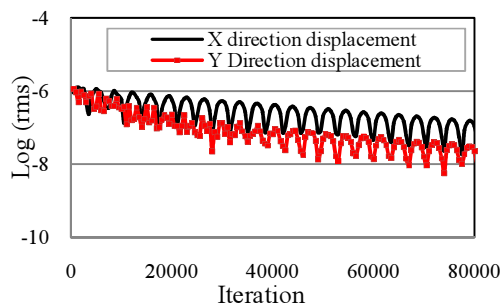
Fig. 21. Convergence of the results for tip displacements

surrounded by the constant temperature liquid is calculated. Second, the stress-strain field of a plate under distributed loads in two directions is solved with developed model on unstructured triangular meshes. Having obtained acceptable results from two modules of the combined solver, the temperature-induced stress-strain field due to external constraints is modeled for a clamped plate under uniform temperature field and promising results is obtained.

The novelties of present combined numerical solver can be listed as follows:

1. An explicit time stepping technique for both thermal and stress-strain analysis on a single unstructured triangular meshes is used.

2. The matrix free Galekin Finite Volume solution is presented to plane stress problem with considerably low computational work load and CPU time consumption.

3. The local time stepping method is used to accelerate the steady state computations.

4. In the presented Finite Volume Method straightforward gradient boundary conditions are developed and applied to impose the thermal gradient boundary conditions (using ambient temperature and thermal fluxes normal to the boundary).

5. The technique for imposing stress-strain boundary condition is straightforward that it only requires specification of displacements at the boundary.

Reference

[1] Springenschmid, R.: 1998. Prevention of Thermal Cracking in Concrete at Early Ages, Taylor & Francis Routledge, London.

[2] Ballim, Y.: 2004. A numerical model and associated calorimeter for predicting temperature profiles in mass concrete, Cement & Concrete Composites 26, 695-703.

[3] Ilc, A., Turk, G., Kavćić, F. and Trtnik, G.: 2009. New numerical procedure for the prediction of temperature development in early age concrete structures, Automation in Construction 18, 849-855.

[4] Singh, I.V.: 2004. A numerical solution of composite heat transfer problems using mesh less method, International Journal of Heat and Mass Transfer 47, 2123-2138.

[5] Arifur Rahman, M., Salam Akanda, M.A.: 2005. Effect of circular hole on the distribution of stresses in a rectangular plate, International Conference on Mechanical Engineering (ICME2005), 1-6.

[6] Taliercio, A.: 2005. Generalized plane strain finite element model for the analysis of elastoplastic composites, International Journal of Solids and Structures 42, 2361-2379.

[7] Atluri, S.N., Liu, H.T. and Han, Z.D.: 2006. Meshless local Petrov-Galerkin (MLPG) mixed collocation method for elasticity problems, CMES 14 (3), 141-152.

[8] Liu, N. and Liu, G.T.: 1996. Spectral stochastic finite element analysis of periodic random thermal creep stress in concrete, Engineering Structures 18 (9), 669-674.

[9] Chen, D.P., Qian, C.X. and Liu, C.L.: 2010. A numerical simulation approach to calculating hygro-thermal deformation of concrete based on heat and moisture transfer in porous medium, International Journal of Civil Engineering 8 (4), 287-296.

[10] Mazloom, M. and Ramezanian Pour, A.A.: 2004. Time-dependent behavior of concrete columns containing silica fume, International Journal of Civil Engineering 2 (1), 23-31.

[11] Omidi, O, and Lotfi, V.: 2010. Finite element analysis of concrete structures using plastic-damage model in 3-D implementation, International Journal of Civil Engineering 8 (3), 187-203.

[12] Vaz Jr, M., Muñoz-Rojas, P.A. and Filippini, G.: 2009. On the accuracy of nodal stress computation in plane elasticity using finite volumes and finite elements, Computers and Structures 87, 1044-1057.

[13] Lyra, P.R.M., Lima, R.D.C.F.D., Guimarães, C.S.C. and Carvalho, D.K.E.D.: 2002. An edge-based unstructured finite volume method for the solution of potential problems, Mecanica Computational XXI, 1213-1231.

[14] Lyra, P.R.M., Lima, R.de C.F.de., Guimarães, C.S.C. and Carvalho, D.K.E.de.: 2004. An edge-based unstructured finite volume procedure for the numerical analysis of heat conduction applications, Journal of the Brazilian Society of Mechanical Sciences and Engineering XXVI (2), 160-169.

[15] Sabbagh-Yazdi S.R. and Bagheri A.R.: 2004. Computer simulation of cement heat generation and temperature profiles in mass concrete structures, International Journal of Engineering Science 15(2), 65-71.

[16] Wheel, M.A.: 1996. A finite-volume approach to the stress analysis of pressurized axisymmetric structures, International Journal of Pressure Vessels and Piping 68, 311-317.

[17] Oliveira, P.J. and Rente, C.J.: 1999. Development and application of a finite volume method for static and transient stress analysis, Proc. NAFEMS World Congress'99 on Effective Engineering Analysis 1, 297-309.

[18] Wenke, P. and Wheel, M.A.: 2003. A finite volume method for solid mechanics incorporating rotational degrees of freedom, Computers and Structures 81, 321-329.

[19] Sabbagh-Yazdi, S.R., AliMohammadi, S.: 2011. Performance evaluation of iterative GFVM on coarse unstructured triangular meshes and comparison with matrix manipulation based solution methods, Journal of Scientia Iranica, 18(2), 131-138.

[20] Demirdzić, I. and Martinović, D.: 1993. Finite volume method for thermo-elasto-plastic stress analysis, Computer Methods in Applied Mechanics and Engineering 109, 331-349.

[21] Demirdzić , I., Horman, I. and Martinovi?, D.: 2000. Finite volume analysis of stress and deformation in hygro-thermo-elastic orthotropic body, Computer Methods in Applied Mechanics and Engineering 190, 1221-1232.

[22] Fainberg, J. and Leister, H.J.: 1996. Finite volume multigrid solver for thermo-elastic stress analysis in anisotropic materials, Computer Methods in Applied Mechanics and Engineering 137, 167-174.

[23] Logan, D.: 2001. A First Course in the Finite Element Method Using ALGOR, Brooks/Cole Pu, California, United States.

[24] Fu, Y.F.: 2003. Thermal Stresses and Associated Damage in Concrete at Elevated Temperatures, Ph.D Thesis, The Hong Kong Polytechnic University, Hong Kong.

[25] Segerlind, L.J.: 1984. Applied Finite Element Analysis, Second Edition, Agricultural Engineering Department, Michigan state University, John Wiley and Sons.

[26] Branco, F.A., Mendes, P. and Mirambell, E.: 1992. Heat of hydration effects in concrete structures, ACI Materials Journal, 89(2), 139-145.

[27] Pitts, D. and Sissom. L.: 1998. Schaum's Outline Heat Transfer, McGraw - Hill, New York.

[28] Beer, F.P. and Johnston, E.R.: 1992. Mechanics of Materials, JR. McGraw-Hill.